Phase stability and mechanical properties of niobium nitrides

V. I. Ivashchenko,[1] P. E. A. Turchi,[2] and E. I. Olifan[1]
[1]*Institute of Problems of Materials Science, NAS of Ukraine, Krzhyzhanovsky Street 3, 03142 Kyiv, Ukraine*
[2]*Lawrence Livermore National Laboratory, L-352, P.O. Box 808, Livermore, California 94551, USA*
(Received 26 April 2010; revised manuscript received 14 June 2010; published 13 August 2010)

First-principles pseudopotential calculations were performed to investigate the structural stability of various phases of niobium nitrides NbN_x. The stability of the NaCl-, NiAs-, AsNi-, and CW (anti–WC)-type NbN phases, the substoichiometric Nb_8N_7, Nb_4N_3, and $Nb_{32}N_{31}$ compounds are analyzed on the basis of the results of electronic structure and phonon calculations. The behavior of these structures under uniaxial tensile strain was investigated. The electronic origin of the soft phonon modes and the mechanical properties of niobium nitrides are discussed.

DOI: 10.1103/PhysRevB.82.054109 PACS number(s): 63.20.dk, 64.60.Ej, 71.15.Nc

I. INTRODUCTION

Let us briefly consider the main experimental results on NbN_x since the structural and physical properties have been amply reviewed in Refs. 1 and 2. It is known that NbN_x can be prepared as powder samples,[3] diffusion couples,[4,5] and films.[6] Given the recent investigations on the Nb-N system,[4,6] the nitrogen-rich NbN_x phases could be classified as follows: (i) δ-NbN_x, $0.72<x<1.06$, with the NaCl-type lattice (space group $Fm\bar{3}m$) exists above T_c $=1070-1225$ °C.[4,5] The nitrogen atoms and vacancies are arranged statistically; (ii) body-centered tetragonal γ-Nb_4N_{3x} or γ-NbN_x, for $0.72<x<0.84$ (space group $I4/mmm$).[5] γ-NbN_x transforms into δ-NbN_x above T_c; (iii) hexagonal ϵ-NbN is described with an anti-WC-type lattice (CW, space group $P\bar{6}m2$).[2] ϵ-NbN is stable below 1330 °C;[5] (iv) hexagonal δ'-NbN_x, $0.95<x<0.98$, with an anti-NiAs-type lattice (AsNi, space group $P6_3/mmc$) (Refs. 4 and 6) is supposed to occur only transiently during the formation of ϵ-NbN from δ-NbN_x. Despite a lot of effort that has been put in classifying and understanding the various phases of the Nb-N system so far the mechanism of the δ-γ transition remains unclear.

The cubic δ-NbN_x phases exhibit relatively high superconducting temperature, at least for this class of materials, that can reach a value of 17.8 K,[1] which makes them suitable for application in low-temperature electronics. Besides this remarkable property, niobium nitrides are characterized by high chemical stability and high hardness.[1,2] Good mechanical properties together with chemical inertness and high melting points make these nitrides suitable materials for protective and wear-resistant coatings.[7,8]

Experimental investigation of the phonon spectra was carried out only for the NaCl-type NbN_x: phonon anomalies around the X point were observed by inelastic neutron-diffraction measurements.[9] The dynamical stability of various structure types of NbN was analyzed in Ref. 10 on the basis of first-principles pseudopotential (PP) calculations of their phonon spectra.

The general trends in the electronic structure properties of NbN_x were summarized in Refs. 10–13. First-principles pseudopotential calculations were carried out to examine polymorphism and metastability in NbN.[14] It was shown that among three structure types, namely, CW, AsNi, and NaCl, the CW-type NbN exhibited the lowest total energy, whereas the cubic phase was energetically the most unfavorable structure. A pseudopotential method was also used to investigate the mechanical properties of the hexagonal and cubic phases of NbN,[15,16] the electronic structure of niobium mononitride surfaces[17,18] and the lattice dynamics of the NaCl-, NiAs-, and WC-types of NbN.[10]

Despite the substantial amount of experimental and theoretical information accumulated on niobium nitrides, some important questions have not been yet addressed. Among them it is worth mentioning the following: (1) there are no theoretical investigations of atomic and electronic structures, lattice dynamics, and stability of various NbN_x phases within a single *ab initio* approach. (2) The mechanism of the δ-γ structural transformation remains so far unclear. (3) In the NiAs structure there are six Ni-As, six As-As, and two Ni-Ni nearest-neighbor bonds; it follows from this that the NiAs and AsNi structures are not identical although, sometimes, these two structures are undifferentiated in the literature.[10,16] Up today, there is no comparative study on phonon-structure and total-energy results for these two structures. (4) It was experimentally established that NbN films with the hexagonal phases (ϵ-NbN, δ'-NbN) exhibit higher hardness than the films based on δ-NbN,[7,8] and no satisfactory explanation has been yet provided.

Therefore, it is highly motivating to focus our attention on these questions. In this work we aim at filling these gaps in studying the physical properties of NbN_x, as well as resolving the contradictions when interpreting the theoretical results on δ'-NbN. For this purpose, we calculated the atomic and electronic structures, total energy, phonon spectra, and stress-strain relations of various structural types of NbN: NaCl, NiAs, AsNi, and CW using the *ab initio* PP method with a plane-wave-basis set. The same procedure was applied to the study of substoichiometric $NbN_{0.97}$ ($Nb_{32}N_{31}$, $Pm3m$), $NbN_{0.875}$ (Nb_8N_7, space group $P4/mmm$), and $NbN_{0.75}$ (Nb_4N_3, space groups $Pm3m$ and $I4/mmm$) structures. Based on these results we analyze phase stability as a function of structure type, composition, and temperature. The stress-strain relation under tensile strain is computed and analyzed, and the results are compared to other available theoretical and experimental data.

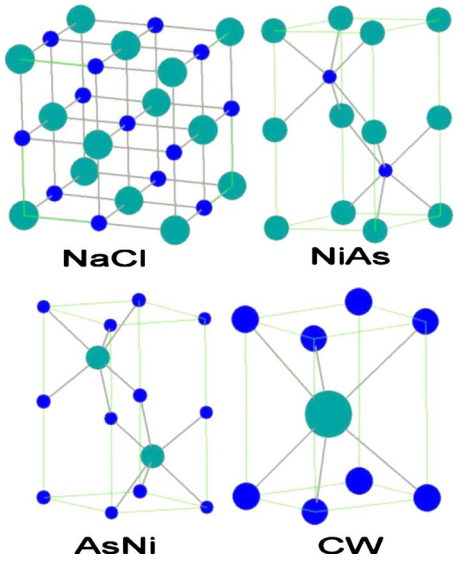

FIG. 1. (Color online) Unit cells of the four NbN structures considered in the present study. Nb—large circles, N—small circles.

The paper is organized as follows. Sec. II is devoted to computational details. The peculiarities of the calculations in the framework of a first-principles PP method applied to the NbN structures are described in details. In Sec. III, the results of the calculations are presented and discussed. Here phonon spectra, total energies, lattice relaxations, electronic spectra, and stress-strain relation of various phases of NbN_x are analyzed. Finally, Sec. IV contains the main conclusions.

II. COMPUTATIONAL DETAILS

Total energy (E_T) calculations within the local-density approximation of density-functional theory were carried out using the QUANTUM-ESPRESSO first-principles code[19,20] for two-atom (NaCl- and CW-type NbN), four-atom (NiAs- and AsNi-type NbN), seven-atom (cubic and tetragonal Nb_4N_3), and 15-atom (tetragonal Nb_8N_7) unit cells. The unit cells of the cubic and hexagonal structures are shown in Fig. 1. The tetragonal supercells consist of two eight-atom NaCl lattices aligned along the z direction with one nitrogen vacancy in the central position (Nb_8N_7) and with two nitrogen vacancies at the origin and in the central position (Nb_8N_6). The latter structure can be represented as a seven-atom tetragonal cell (Nb_4N_3, $I4/mmm$) with "antiparallel" vacancy ordering. The cubic seven-atom Nb_4N_3 cell ($Pm3m$) with one nitrogen vacancy in the central position represents a structure with parallel vacancy ordering. The 63-atom NaCl-type (2 2 2) supercell was used to model the $Nb_{32}N_{31}$ structure. All these structures were relaxed. Vanderbilt ultrasoft pseudopotentials were used to describe the electron-ion interaction.[21] In this approach, the orbitals are allowed to be as soft as possible in the core regions so that their plane-wave expansion converges rapidly.[21] The semicore states were treated as valence states. For the niobium pseudopotential, nonlinear core corrections were taken into account.[19] To describe the exchange-correlation energy, the generalized gradient approximation (GGA) (Ref. 22) was considered. The criterion of convergence for the total energy was 10^{-6} Ry/f.u. To speed up convergence, each eigenvalue was convoluted with a Gaussian with a width σ=0.02 Ry. The cut-off energy for the plane-wave basis was set to 38 Ry. Since we dealt with different structures, a similar setup was used for basis set, tail energies, and k-point mesh. The integration in the Brillouin zone (BZ) was performed with a set of special k points determined according to the Monkhorst-Pack scheme[23] using a (8,8,8) mesh. The band structure of $Nb_{32}N_{31}$ was computed using only the Γ point. The density of states (DOSs) was calculated with the tetrahedron method using a (12, 12, 12) mesh.[19]

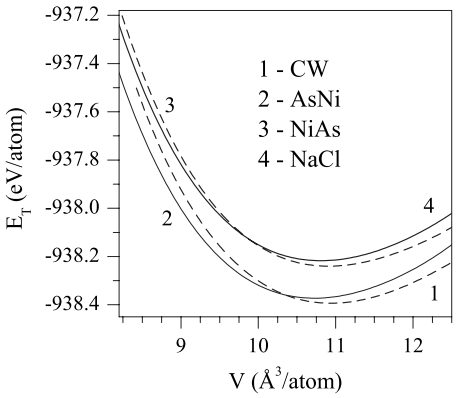

FIG. 2. Total energy versus cell volume for various structural forms of NbN.

The equilibrium geometry of each structure under consideration (except for the stoichiometric NaCl-type NbN) was determined by considering the simultaneous relaxations of the ions and the unit cells without preserving the symmetry with a Parinello-Rahman method.[24] Relaxation of the atomic coordinates and of the unit cell was considered complete when atomic forces were less than 1.0 mRy/bohr, stresses were smaller than 0.05 GPa, and total energy during the structural optimization iterative process was changing by less than 0.1 mRy.

The calculations of the bulk modulus B and its pressure derivative were achieved by changing the cell volume of the computed structures about their equilibrium geometry, and fitting the energy-volume data to the Murnaghan equation of states.

The tensile stress (σ_{zz}) was found in the following way. A unit cell was elongated along the z direction in incremental steps. For the hexagonal structures, the z direction was aligned with the c-basis vector. For each increment the total energy and the relaxed cell volume (V) were calculated. The stress was determined as the derivative of the total energy with respect to the tensile strain (ϵ_{zz}), $\sigma_{zz}=(1/V)\,\partial E_T/\partial\epsilon_{zz}$. The QUANTUM-ESPRESSO first-principles code was used to calculate the phonon spectra of cubic and hexagonal NbN in the framework of density-functional perturbation theory.[19,25]

III. RESULTS AND DISCUSSION

A. Total energy calculations

First, we calculated the total energies of the stoichiometric cubic and hexagonal phases of NbN as functions of cell vol-

TABLE I. Lattice parameters (a, c/a), bulk moduli (B) and their derivatives (B') obtained in this work, together with results from other theoretical studies (parenthesis) and experiments (curly brackets).

Phase	Symmetry (space group)	A (Å)	c/a	B (GPa)	B' (GPa)
NaCl	Cubic	4.422[a]	1.00[a]	302[a]	4.2[a]
	($Fm\bar{3}m$)	(4.37[b], 4.41[c])		(313[c],314[f])	
		(4.378–4.42[d])		(309–354[d])	
		{4.391[e]}		{287,292,354[d]}	
NiAs	Hexagonal	2.939[a]	1.99[a]	300[a]	4.1[a]
	($P6_3/mmc$)	(2.930[c])	(1.99[c])	(310[c],311[f])	
AsNi	Hexagonal	2.98[a]	1.87[a]	312[a]	3.9[a]
	($P6_3/mmc$)	(2.953[b])	(1.86[b])		
		{2.968[e]}	{1.87[e]}		
CW	Hexagonal	2.962[a]	0.97[a]	308[a]	4.1[a]
(WC)	($P\bar{6}m2$)	(2.928[b],2.958[g])	(0.97[b],0.97[g])		
		{2.94[e]}	{0.95[e]}		
Nb_8N_7	Tetragonal	4.410[a]	1.98[a]	292[a]	4.3[a]
	($P4/mmm$)				
Nb_4N_3	Cubic	4.382[a]	1.00[a]	280[a]	4.4[a]
	($Pm3m$)				
Nb_4N_3	Tetragonal	4.396[a]	1.97[a]	283[a]	4.1[a]
	($I4/mmm$)	{4.382[h]}	{1.97[h]}		

[a](PP-GGA) This work.
[b](PP-LDA) Ref. 14.
[c](PP-GGA) Ref. 16.
[d]Review given in Ref. 10.
[e](Handbook) Ref. 3.
[f]PP-GGA) Ref. 7.
[g](PP-GGA) Ref. 18.
[h](XRD) Ref. 26.

ume. The results of these calculations are shown in Fig. 2 and the structural characteristics of the calculated phases are summarized in Table I. One can note from Table I that the computed lattice parameters for these structures are in fairly good agreement with those obtained from other theoretical and experimental investigations. Figure 2 shows that there are two hexagonal phases of NbN, CW, and AsNi, which are stable at various pressures at zero temperature. In Fig. 3 we show the enthalpy and cell volume of the CW- and AsNi-type structures of NbN as functions of pressure. It is seen that the CW structure is stable at pressures below 13.5 GPa. At higher pressures, this structure transforms into the AsNi phase. Stoichiometric niobium nitride cannot be stable in the cubic NaCl and hexagonal NiAs structures at any pressures. The differences in the ground-state energies between the CW-type NbN and the other three structures are 0.021, 0.153, and 0.177 eV/atom for the AsNi, NiAs, and NaCl structural types, respectively.

B. Dynamical properties

Another way to study structural stability of crystalline materials is to analyze the lattice dynamic properties since the existence of soft phonon modes indicates structural instability. We calculated the phonon dispersion curves along the symmetry directions in the BZ for the four structural types of NbN considered above. The computed phonon spectra are presented in Figs. 4–7. There are no phonon anomalies that could lead to the instability of hexagonal CW and AsNi. For NiAs, a soft mode at the M point was identified. This soft mode approaches zero under uniaxial compression [cf. Fig. 6(b)], which indicates a dynamical instability of the NiAs structure with respect to small distortions. In the case of the NaCl-type structure, we find imaginary acoustic frequencies at the X point (longitudinal, $X_{3'}$, and transverse, $X_{5'}$), which is incompatible with the dynamical stability of this phase [cf. Fig. 7(a)]. These phonon anomalies arise because of electronic transitions between the $W_{3'}$ states that strongly increase a negative contribution to the dynamical matrix for the phonon wave vector X.[27]

A comparison of the phonon dispersion curves for the NaCl- and CW-type structures of NbN with those calculated in Ref. 10 shows that both calculations give similar results. For the ground state of NiAs-type NbN, the phonon spectrum[10] has an imaginary frequency near the M point. According to our results, the collapse of the acoustic mode at the M point occurs only under uniaxial compression [cf. Fig. 6(b)]. Unfortunately, we cannot explain this discrepancy

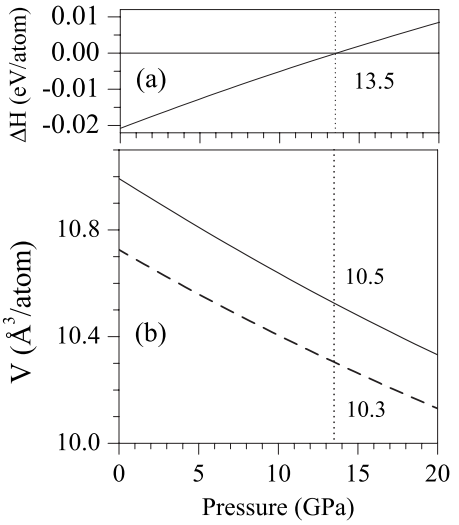

FIG. 3. (a) Enthalpy difference $\Delta H = H(\mathrm{CW}) - H(\mathrm{AsNi})$, and (b) cell volume of the CW-(solid line) and AsNi-(dashed line) type structures of NbN as a function of pressure. The numbers refer to the transition pressure in (a) and the cell volumes in (b).

since we have no information on the structural parameters used in the calculations of Ref. 10.

Let us now analyze the effect of temperature and small concentrations of nitrogen vacancies on the phonon spectrum of δ-NbN. In NaCl-type NbN_x, with small deviations from the stoichiometry, atoms and vacancies in the nonmetal sublattice are randomly distributed.[1] For the band-structure study of such random systems, usually one uses the coherent potential approximation (CPA). The Korringa-Kohn-Rostoker-CPA energy band calculations of NbN_x (Ref. 12) showed that, for small vacancy composition, the dangling-bond states are located in a minimum of the density of states, below the Fermi energy E_F, and the main effect of disorder on band energies around E_F was a band smearing and a lowering of the Fermi level. It is well known also that, to a first-order approximation, temperature effect results in a smearing of the band energies. To account for the effects of temperature and nitrogen vacancies on the phonon spectrum of NbN_x, we calculated the phonon-dispersion curves by using various values of band-energy smearing σ. To substantiate the hypothesis of an acoustic mode softening around the X point that occurs with a decrease in temperature and an increase in nitrogen composition, x, in NbN_x, we calculated

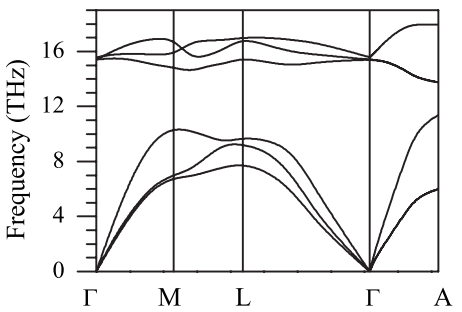

FIG. 4. Calculated dispersion phonon curves for CW-type NbN.

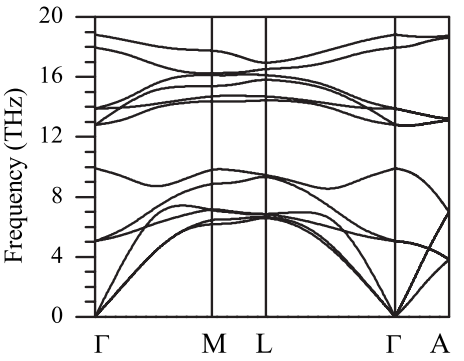

FIG. 5. Calculated dispersion phonon curves for AsNi-type NbN.

the dispersion curves along high-symmetry directions for two values of the smearing parameter, $\sigma = 0.02$ and 0.16 Ry. These phonon spectra are displayed in Fig. 7. An increase in σ, that implies an increase in temperature and nitrogen vacancies, leads to the disappearance of the phonon anomalies, and a better agreement between calculated and experimental spectra[9] is achieved [cf. Fig. 7(b)]. This finding validates fairly well our approximations. In Figs. 8(a) and 8(b), we show the effect of band-energy smearing σ on the position of E_F with respect to the $W_{3'}$ level and the frequencies of the soft modes in NaCl-type NbN. As σ increases, the Fermi level gradually moves toward lower energies crossing the $W_{3'}$ level. Owing to the lowering of the Fermi level and an increase in σ the frequencies of the soft $X_{3'}$ and $X_{5'}$ acoustic phonons increase, and the cubic structures of NbN_x are stabilized. These results show that δ-NbN_x can form with the NaCl-type structure only at high temperatures ($x = 1.0$) or with a deficiency in nitrogen atoms ($x < 1.0$) at low temperatures.

C. Structural stability and lattice relaxation

We also applied this simple approach to examine the structural stability of various phases of NbN_x. For this purpose, the total energies of the CW, AsNi, NiAs, and NaCl

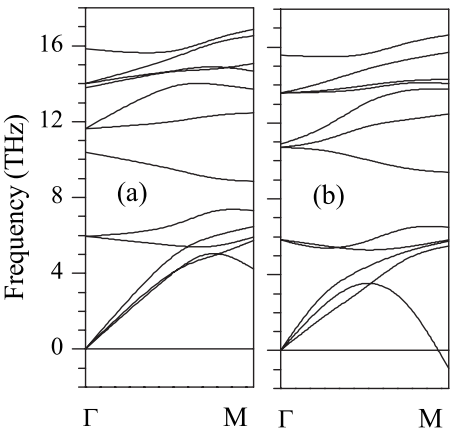

FIG. 6. (a) Calculated dispersion phonon curves along the Γ-M line for NiAs-type NbN at equilibrium and (b) under uniaxial compression ($\varepsilon_{zz} = 0.03$).

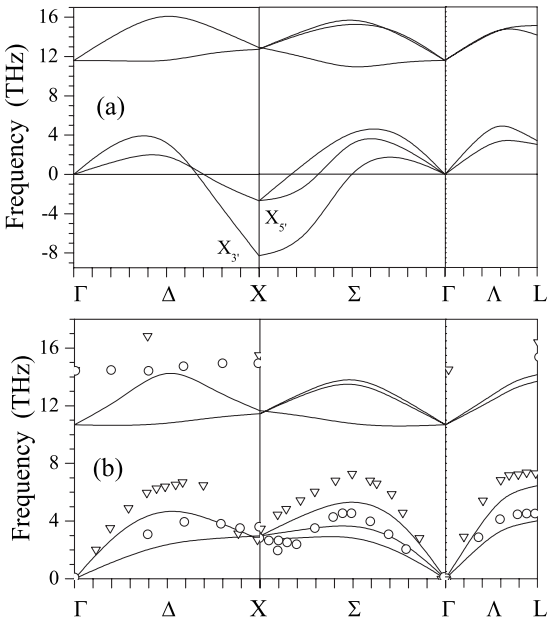

FIG. 7. Calculated dispersion phonon curves for NaCl-type NbN for (a) σ=0.02 Ry and (b) σ=0.16 Ry. The triangles and circles in (b) represent the experimental spectrum for $NbN_{0.93}$ (Ref. 9).

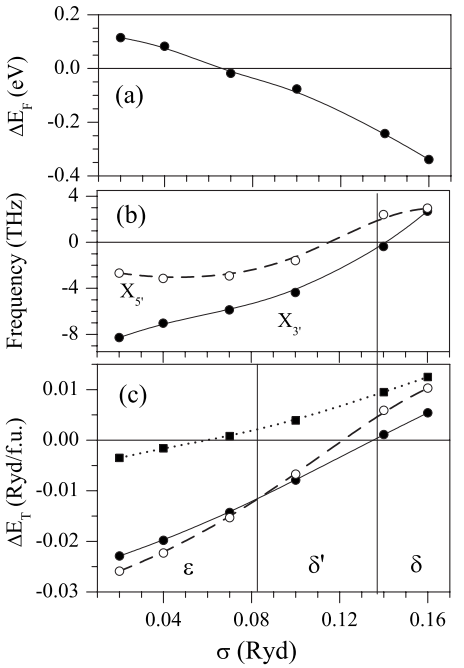

FIG. 8. (a) Energy difference $\Delta E_F = E_F - E(W_{3'})$, (b) phonon frequencies of the soft modes in the NaCl-type NbN, and total energy differences $\Delta E_T = E_T(\mathrm{CW}) - E_T(\mathrm{NaCl})$ (open circles), (c) $\Delta E_T = E_T(\mathrm{AsNi}) - E_T(\mathrm{NaCl})$ (solid circles) and $\Delta E_T = E_T(\mathrm{NiAs}) - E_T(\mathrm{NaCl})$ (full squares) as functions of band energy smearing σ.

structure types were calculated as functions of σ. The results of the total-energy calculations are presented in Fig. 8(c). They predict the following sequence of phase transformations with increasing σ: $\varepsilon \rightarrow \delta' \rightarrow \delta$. One should note that the δ-NbN_x phases only appear after the soft $X_{3'}$ phonon mode becomes positive. As a reminder, the ε-NbN phase practically does not contain nitrogen vacancies, and δ'-NbN_x has a very narrow homogeneity range.[1,4,6] This means that the obtained sequence of phase transformations will occur in NbN_x, for $x \sim 1.0$, with increasing temperature. It is seen that the δ' phase is the intermediate one in this sequence of phase transformations, which is consistent with experiment.[4] NiAs-type NbN is found to be energetically unfavorable over the whole range of σ. Hence, it clearly follows that the NiAs and AsNi structure types of NbN should not be confused, and only AsNi-type NbN should be identified with the δ'-NbN phase, in agreement with experiment.[4]

We considered above the NbN_x structures with negligible concentrations of nitrogen vacancies. It is well known that only the tetragonal γ-NbN_x and cubic δ-NbN_x phases exist in a wide composition range.[3–6] The cubic δ-NbN_x to tetragonal γ-NbN_x transition occurs below the transition temperature, $T_c \sim 1070-1225$ °C.[5] Assuming that this transition could be initiated by lattice relaxation around nitrogen vacancies, we analyzed the static atomic displacements around a single nitrogen vacancy. We considered the cubic $Nb_{32}N_{31}$ structure for σ=0.02 Ry. It was found that the niobium atoms relax tetragonally inward with $u_x = u_y = 0.136$ Å and $u_z = 0.156$ Å. We suspect that the inward lattice relaxation is related to a predominance of the repulsive Nb-N pair interactions. Here it should be noted that in TiC_x, NbC_x, and TiN_x, outward relaxations are observed,[28] which speaks in favor of a predominance of attractive metal-nonmetal pair interactions. The tetragonal character of the atomic displacements is assumed to be caused by the split of the double-degenerated Γ_{12} level that occurs in the vicinity of the Fermi level (cf. Fig. 11 below). The reason why a tetragonal distortion can explain a split of these levels can be easily shown by using the invariant method.[29] According to this scheme,[29] only the tetragonal strains are able to split the double-degenerated Γ_{12} level. It follows that the formation of the ordered tetragonal γ-$NbN_{0.75}$ structure could be caused by lattice relaxations around the nitrogen vacancies. However, this is not the case. As will be shown below, this structure is instead stabilized by a specific vacancy ordering.

In substoichiometric transition-metal carbides and nitrides, a reduction in temperature leads, as a rule, to the formation of ordered structures.[28] In the case of NbN_x, such structures are observed for compositions close to x=0.75.[5,26] At such compositions, two types of vacancy ordering are possible: parallel and antiparallel.[28] The parallel type is realized in $NbC_{0.75}$.[28] To examine the possible formation of both structures in $NbN_{0.75}$, we performed total-energy calculations of the unrelaxed cubic ($Pm3m$) and tetragonal ($I4/mmm$) Nb_4N_3 phases. We found that the total energy of the cubic phase is greater than that of the tetragonal phase by 0.025 eV/atom. The relaxation of the tetragonal structures reduces E_T only by 0.003 eV/atom. These findings show that in $NbN_{0.75}$ the antiparallel vacancy ordering is preferred, and the small total-energy contribution related to lattice relaxations indicates that vacancy ordering is a driving force for the formation of the ordered γ-$NbN_{0.75}$ phase.

To study lattice relaxation around a nitrogen vacancy in the tetragonal structures we calculated the atomic configurations of NbN_x, for x=0.875 (Nb_8N_7) and 0.75 (Nb_4N_3) by allowing relaxation of the cells and atomic positions. It was

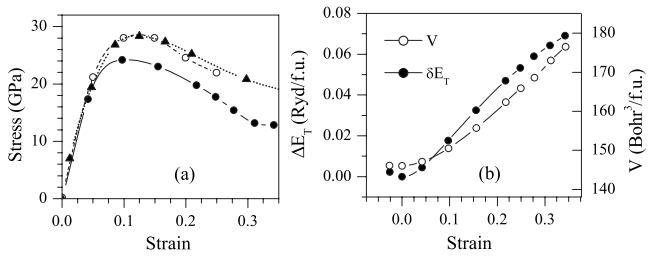

FIG. 9. Calculated stress versus tensile strain for the (001) stress in NaCl-type NbN (full circles), Nb_4N_3 (full triangles), and NaCl-type NbN obtained by Wang *et al.* (Ref. 16) (open circles). Total energy difference between strained and unstrained NaCl-type NbN, $\delta E_T = E_T(\varepsilon) - E_T(0)$, (full circles) and cell volume (open circles) as functions of strain ε (b).

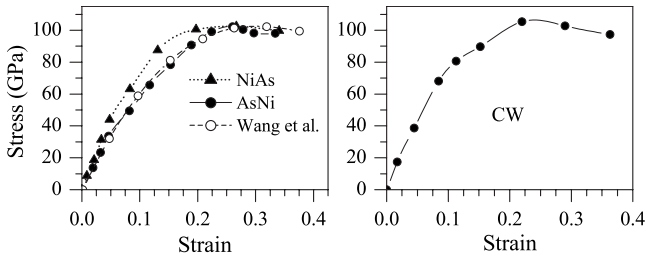

FIG. 10. Calculated stress versus strain for the (0001) stress in various hexagonal structures of NbN. For the sake of comparison, the corresponding data for NiAs-type NbN calculated by Wang *et al.* (Ref. 16) are also presented.

found that the bulk modulus, lattice parameter (a) and ratio c/a for NbN_x decrease as x decreases (cf. Table I). These changes reproduce fairly well the trend in the behavior of the mechanical and structural properties of NbN_x with composition x.[1,4] In both computed tetragonal structures, two of the six niobium atoms in the neighborhood of a nitrogen vacancy shift toward the vacancy site along the z direction, in contrast to other similar compounds such as, for example, TiC_x and TiN_x, where in these cases the metal atoms relax outward.[28,30] For the composition $x=0.875$, the inward relaxation of 0.033 Å inside the tetragonal supercell leads to the formation of a primitive tetragonal structure (space group $P4/mmm$) with $c/a<1.983$. For $NbN_{0.75}$, although the inward relaxation does not violate the symmetry of the initial body centered tetragonal cell (space group $I4/mmm$), it leads to a reduction in the c/a ratio to 1.968. In this case, the niobium atoms shift by 0.047 Å, which is close to the experimental value of 0.036 Å.[26] Note that the value of the atomic shift depends on the symmetry and the composition of the substoichiometric phases.

D. Mechanical properties

In theoretical studies, one often considers the bulk modulus and the flow stress (the critical stress at which the ideal crystal becomes structurally unstable) as indicators of the intrinsic material strength.[16] In addition, theoretical investigations of the stress-strain relations give a deeper understanding of material behavior under large strains. We calculated the stresses of all four structures of NbN and Nb_4N_3 as functions of uniaxial tensile strain. In Figs. 9 and 10, the calculated stress-strain curves are displayed. To show the effect of tensile load on total energy and cell volume, in Fig. 9(b) we present these characteristics as functions of tensile strain. The calculated stress-strain curves exhibit an elastic behavior at small strains. At large strains, the stress exhibits different behaviors for various NbN_x structures. In particular, for cubic NbN and tetragonal Nb_3N_4, the stress reaches a maximum value of 24 GPa and 28 GPa at a strain of about 0.1 and 0.13, respectively. The flow stress increases from the stoichiometric cubic NbN to the substoichiometric tetragonal $NbN_{0.75}$. In the case of the hexagonal phases, the flow stresses, determined at $\varepsilon \sim 0.25$, are about 102 GPa (NiAs-type and AsNi-type NbN) and 107 GPa (CW-type NbN). The flow stresses and critical strains for the hexagonal phases are larger as compared to those for the cubic and tetragonal phases. It was found that, for Cu,[31] the relaxed structures had lower total energies than the unrelaxed ones. Following this finding, we expected that our values of the flow stresses would be overestimated. However, the comparison of the results for the relaxed and nonrelaxed δ-NbN structures presented in Fig. 9(a) clearly indicates that not only the atomic relaxations influence the stress-strain curves but also different conditions for the calculations in the framework of the same approach can lead to different results. Unfortunately, we did not find any experimental stress-strain relations for the NbN structures to verify our calculated data. Nevertheless, assuming that the effect of atomic relaxations on the mechanical behavior of various NbN phases under tensile stress will be of the same order, a comparative analysis of the calculated stress-strain relations would be justified. Based on such an analysis, we predict that ε-NbN and, and to a lesser extent δ'-NbN will have the highest flow stresses among all the NbN structures, which makes them materials with promising industrial and technological applications.

E. Electronic structure properties

It is well known that, in most cases, the peculiarities of the electronic structure determine the mechanical properties of materials. We calculated the electronic band structures and densities of states of various phases of NbN_x to acquire a better understanding of the mechanical properties of these phases. The electronic band structures of various phases of NbN are displayed in Fig. 11. In Fig. 12 we show the calculated DOSs with comparison to the experimental x-ray photoelectron spectra (XPS) (Ref. 32) and a previous theoretical electronic spectrum for NiAs-type NbN.[16] All the electronic spectra exhibit three main bands. A detailed analysis of the partial DOSs (not presented here) shows that the low-energy band originates from the N $2s$ state. The next d-p band located around −5 eV is mostly associated with the Nb d and N p states. In δ-NbN, the d-p band does not split, whereas in the case of the hexagonal structures it splits into two subbands related to the (Nb d-N p)σ and (Nb d-N p)π bonds. Because of the structural peculiarities of the hexagonal phases, the (Nb d-N p)σ bonds are directed mainly along the c axis and the (Nb d-N p)π bonds are distributed mainly in

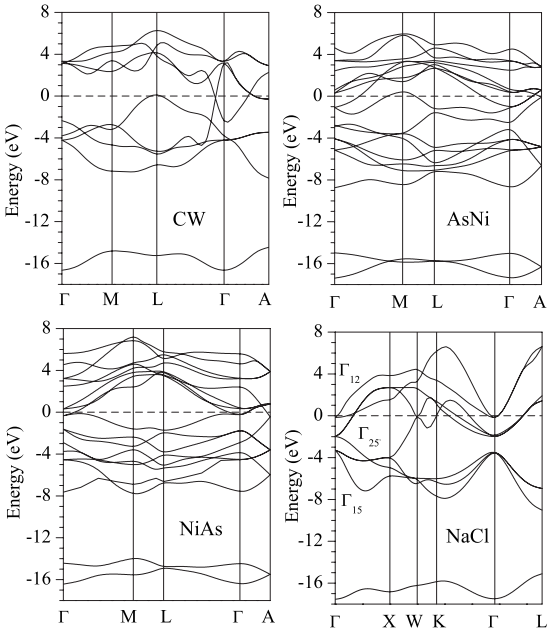

FIG. 11. Electronic band structures of various structural forms of NbN. For the band structure of the NaCl-type NbN, the states at the Γ point are indicated. The horizontal lines locate the Fermi level.

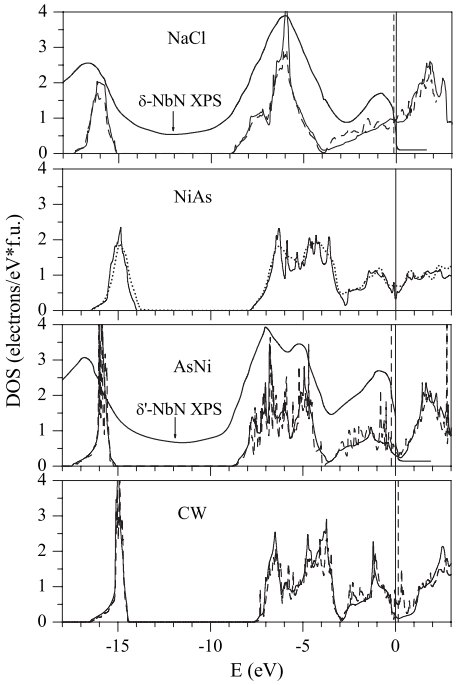

FIG. 12. Calculated DOSs of various unrelaxed structures of $NbN_{1.0}$ (solid line) and $NBN_{0.875}$ (Nb_8N_7) (dashed line). For comparison, the XPS for δ-NbN and δ'-NbN (Ref. 32) and the DOS of NiAs-type NbN calculated by Wang *et al.* (Ref. 16) (dotted line) are also presented. The vertical solid and dashed lines locate the Fermi energies in $NbN_{1.0}$ and $NbN_{0.875}$, respectively.

the plane that is perpendicular to the c axis. The band related to the (Nb d-N p)σ bonds are shown in the DOS in the low-energy region. It is these bonds that contribute most to the extremely high strength along the (0001) direction.[16] Finally, the high-energy metallic d band is located below and above the Fermi level. Because of the strong Nb d-N p interaction, this band splits into a low-energy Nb d_ε subband and a high-energy Nb d_γ subband. In the case of NaCl-type NbN, the Fermi level is located below the DOS minimum that separates these subbands, whereas in the AsN-type and CW-type NbN, E_F is locating right in this minimum of the DOS. Furthermore, the states of the Nb d subbands in the hexagonal phases are strongly localized, which indicates the high extent of the covalent nature of the metal bonds. The latter points to a strengthening of the metallic bonds in the hexagonal phases compared to what is found for the cubic structure. The strong localization of the states that form the Nb d subbands in the CW-type NbN is also expected to be responsible for the highest value of the flow stress among all the hexagonal structures.

Why is NiAs-type NbN high in energy compared to other hexagonal phases? Given the peculiarities of all the electronic spectra presented in Fig. 12, we see that the states of the d band in NiAs-type NbN are less strongly localized than those in AsNi- and CW-type NbN. As a result, for NiAs-type NbN, the DOS at the Fermi level, N(E_F), is the highest, and the covalent nature of the bonding between the metal atoms is the smallest. Hence, we expect that these two features of the electronic structure reduce the stability of NiAs-type NbN compared to other hexagonal structures.

The comparison between the theoretical and experimental photoelectron spectra for δ-NbN and δ'-NbN, shown in Fig. 12, indicates a fairly good agreement. We note that the XPS of δ'-NbN better agrees with the DOS of AsNi-type NbN than with the electronic spectrum of NiAs-type NbN, an observation which, once again, confirms that δ'-NbN should be identified only with AsNi-type NbN. Figure 12 shows that, for NiAs-type NbN, the DOSs calculated in Ref. 16 and in our work are in excellent agreement.

So far, we did not attempt to explain the various ranges of composition of the NbN_x structures under consideration. To answer this question let us analyze the calculated DOSs of the substoichiometric phases in comparison with those of the stoichiometric ones. The calculated spectra are presented in Figs. 12 and 13. All the substoichiometric phases were calculated without allowing for atomic relaxations, except for the NaCl-based NbN_x structures: these phases were calculated with full relaxations of both the atomic positions and the unit cells. It follows from Fig. 13 that the relaxations do not change the main features of the DOS of the substoichiomentric phases. We note that nitrogen vacancies give rise to additional states below the Fermi level (δ-NbN_x), just below E_F (δ'-NbN_x) and just at E_F (ε-NbN_x). These states originate from the Nb-Nb bonds passing through a nitrogen vacancy. Below, we will attempt to estimate the stability of the substoichiometric structures, following the simple rule: the lower the density of states at the Fermi level, the more stable the structure is. The motivation of this is that the high DOS at E_F causes the existence of soft phonon modes in the long-wave region and their collapse leads to a structural transformation. So, the analysis of phase stability will be done at the level of the correlation between the DOS at E_F and phase stability. For δ-NbN_x, a reduction in x leads to a lowering of E_F and

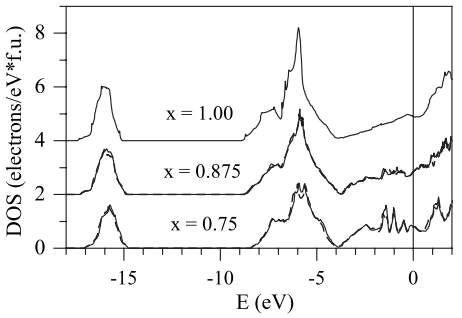

FIG. 13. Calculated DOSs for NaCl-type NbN_x, $x=1.0$ (NbN), $x=0.875$ (Nb_8N_7), and $x=0.75$ (Nb_4N_3). For the substoichiometric compositions, the solid and dashed lines correspond to the DOSs of the relaxed and unrelaxed structures, respectively. The vertical line locates the Fermi energy. The DOSs of different compositions were shifted by aligning the Fermi energies.

$N(E_F)$, which promotes a stabilization of these structures. The decrease in these characteristics continues up to $x=0.7-0.75$ (cf. Fig. 13). By further reducing x, $N(E_F)$ increases, thereby causing a decrease in the stability of the system. This effect explains to a large extent the lower limit for the region of homogeneity of δ-NbN_x and γ-NbN_x. Here it should be noted that the similar band structure changes were observed also for substoichiometric disordered NaCl-type NbN_x.[12] In the case of the AsNi-type NbN_x, a small deviation from stoichiometry leads to a shift of the Fermi level toward the peak of DOS related to "vacancy states" and to an increase in the DOS at the Fermi level (cf. Fig. 12). As a result, δ'-NbN is predicted to be stable only in a very narrow homogeneity range.[3,4] For CW-type NbN, a small number of nitrogen vacancies will give rise to vacancy states just at the Fermi level. Therefore even a single nitrogen vacancy will be able to bring this system into a metastable state. This accounts for the absence of a homogeneity range for ε-NbN.[1–5]

Coming back to the nature of vacancy ordering in NbN_x, let us compare the DOSs of the cubic ($Pm3m$) and tetragonal ($I4/mmm$) $NbN_{0.75}$ phases. The DOSs of these structures are shown in Fig. 14. First, we note that the difference between the band energy contributions to the total energy, $\Delta E_B = E_B(Pm3m) - E_B(I4/mmm)$, where E_B is the integral of the $EN(E)$ function up to $E_F=0.0$ [$N(E)$ is the DOS], is equal to 0.232 eV/atom. The comparison of this value with the total energy difference of 0.025 eV/atom, determined in Sec. III C, prompts us to conclude that the changes in the valence band structure is responsible for the formation of the tetragonal γ-$NbN_{0.75}$ structure caused by vacancy ordering. One can see from Fig. 14 that there are several features in the DOS of the $I4/mmm$ structure that reduce E_B compared to that of the Pm3m phase. These are the DOS peaks at ~ -7, -6, and -2 eV. The first two peaks belong to the Nb d-N p band, whereas the latter peak is formed by the states of the Nb d band. There are two (two) Nb atoms with two (one) neighboring vacancies in the $I4/mmm$ structure and three Nb atoms with two neighboring vacancies and one Nb atoms with an octahedral surrounding in the $Pm3m$ structure. Based on these data, we predict that the (Nb d-N p)σ bonds in the latter structure are weaker than those in the tetragonal phase. The weakening of these bonds is not compensated by a strengthening of the direct (Nb d-Nb d)σ interactions. Such a difference in chemical bonding between these structures can be one possible reason why in the cubic phase the band energy is higher than in the tetragonal structure.

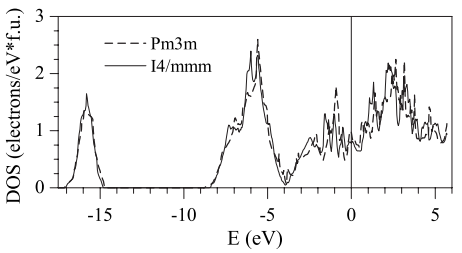

FIG. 14. Calculated DOSs of the unrelaxed NaCl-type $NbN_{0.75}$ structures (Nb_4N_3) with the parallel ($Pm3m$) and antiparallel ($I4/mmm$) vacancy ordering. The vertical line locates the Fermi energy.

In conclusion, we note that our studies based on band-energy smearing have a semiquantitative character since it was possible to correlate in a phenomenological way the smearing parameter σ to temperature and vacancy composition: "an increase in σ implies a corresponding increase in temperature or vacancy composition." Of cause, the investigation of phase stability at finite temperatures should be based on a comparison of the Gibbs free energies of different systems. Nevertheless, such an approach coupled with calculations on equilibrium atomic configurations of stoichiometric phases allowed us to rather correctly describe the main features of the complex phase transformations that take place in NbN.

IV. CONCLUSIONS

First-principles band-structure and phonon-spectrum calculations were performed for various structures of NbN_x. The main results can be summarized as follows: (a) the CW (ε), AsNi (δ'), and NiAs, structure types of NbN are dynamically stable phases. The NaCl-type NbN (δ) is a dynamically unstable phase because of imaginary phonon frequencies around the X point. (b) A simple approach based on a band-energy smearing parameter σ was applied to the description of the structural transformations occurring in NbN_x as functions of temperature and nitrogen-vacancy concentration. This model predicts two phase transitions, $\varepsilon \rightarrow \delta' \rightarrow \delta$, in NbN_x, for $x \sim 1.0$. (c) For $NbN_{0.75}$, the antiparallel vacancy ordering cause a reduction in the total energy by 0.025 eV/atom in comparison to that of the structure with parallel vacancy ordering. This antiparallel vacancy ordering is responsible for the formation of the tetragonal γ-$NbN_{0.75}$ phase, and the small tetragonal lattice distortion arises in the ordered unrelaxed γ-$NbN_{0.75}$ structure due to the relaxation of the stress caused by vacancy ordering. The occurrence of this tetragonal distortion preserves the symmetry of the unrelaxed ordered structure ($I4/mmm$). (d) The NiAs-type NbN is found to be energetically unfavorable compared to other structure types of NbN. It follows that only AsNi-type NbN should be identified with the δ'-NbN phase that is experi-

mentally observed. (e) For the calculated $Nb_{32}N_{31}$, Nb_8N_7, and Nb_4N_3 compounds, inward tetragonal relaxation of the niobium atoms in the neighborhood of a single nitrogen vacancy takes place. (f) The calculated stress-strain relations for the NbN phases indicate that ε-NbN and, to a less extent δ'-NbN, will have the highest flow stresses among all the NbN structures under consideration, and this makes them excellent candidate materials for technological and industrial applications. The promising mechanical characteristics of ε-NbN and δ'-NbN are explained by the strong (Nb d-N p)σ bonds and the strong localization of the Nb d states in the metal band. (g) Nitrogen vacancies in ε-NbN_x and δ'-NbN_x give rise to "vacancy states" at the Fermi level and this leads to a drastic increase in the density of states at the Fermi level and to a destabilization of these phases. Therefore the hexagonal phases have much narrower homogeneity ranges than the cubic and tetragonal defected phases, for which vacancy states appear below the Fermi level.

ACKNOWLEDGMENTS

This work was supported by the STCU under Contract, No. 4682. The work of P.T. was performed under the auspices of the U.S. Department of Energy by the Lawrence Livermore National Laboratory under Contract No. DE-AC52-07NA27344.

[1] L. E. Tot, *Transition Metal Carbides and Nitrides* (Academic, New York, 1971).
[2] G. Brauer, R. Esselborn, and Z. Anorg, *Pearson's Handbook of Crystallographic Data for Intermetallic Phases* (American Society of Metals, Metals Park, OH, 1985).
[3] G. Brauer and R. Esselborn, Z. Anorg. Allg. Chem. **309**, 151 (1961).
[4] R. W. Guard, J. W. Savage, and D. G. Swarthout, Trans. AIME **239**, 643 (1967).
[5] W. Lengauer, M. Bohn, B. Wollen, and K. Lisak, Acta Mater. **48**, 2633 (2000).
[6] M. Benkahoul, E. Martinez, A. Karimi, R. Sanjines, and F. Levy, Surf. Coat. Technol. **180-181**, 178 (2004).
[7] M. Wen, C. Hu, C. Wang, T. An, Y. Su, Q. Meng, and W. Zheng, J. Appl. Phys. **104**, 023527 (2008).
[8] G. Fontalvo, V. Terziyska, and C. Mitterer, Surf. Coat. Technol. **202**, 1017 (2007).
[9] A. Christensen, O. Dietrich, W. Kress, W. Teuchert, and R. Currat, Solid State Commun. **31**, 795 (1979).
[10] E. Isaev, S. Simak, I. Abrikosov, R. Ahuja, Y. K. Vekilov, M. Katsnelson, A. Lichrenstein, and B. Johansson, J. Appl. Phys. **101**, 123519 (2007).
[11] T. Amriou, B. Bouhafs, H. Aourag, B. Khelifa, S. Bresson, and C. Mathieu, Physica B **325**, 46 (2003).
[12] P. Marksteiner, P. Weinberger, A. Neckel, R. Zeller, and P. H. Dederichs, Phys. Rev. B **33**, 6709 (1986).
[13] V. A. Gubanov, A. L. Ivanovsky, and V. P. Zhukov, *Electronic Structure of Refractory Carbides and Nitrides* (Cambridge University Press, Cambridge, 1994).
[14] S. Öğüt and K. M. Rabe, Phys. Rev. B **52**, R8585 (1995).
[15] Z. Wu, X.-J. Chen, V. V. Struzhkin, and R. E. Cohen, Phys. Rev. B **71**, 214103 (2005).
[16] C. Wang, W. Wen, Y. Su, L. Xu, C. Qu, Y. Zhang, L. Qiao, S. Yu, W. Zheng, and Q. Jiang, Solid State Commun. **149**, 725 (2009).
[17] K. Kobayashi, Surf. Sci. **493**, 665 (2001).
[18] I. M. Iskandarova, A. A. Knizhnik, B. V. Potapkin, A. Safonov, A. Bagaturyants, and L. Fonseca, Surf. Sci. **583**, 69 (2005).
[19] S. Baroni *et al.*, http://www.pwscf.org/
[20] S. Scandolo, P. Giannozzi, C. Cavazzoni, S. Gironcoli, A. Pasqurello, and S. Baroni, Z. Kristallogr. **220**, 574 (2005).
[21] D. Vanderbilt, Phys. Rev. B **41**, 7892 (1990).
[22] J. P. Perdew, K. Burke, and M. Ernzerhof, Phys. Rev. Lett. **77**, 3865 (1996).
[23] H. J. Monkhorst and J. D. Pack, Phys. Rev. B **13**, 5188 (1976).
[24] M. Parrinello and A. Rahman, Phys. Rev. Lett. **45**, 1196 (1980).
[25] S. Baroni, S. de Gironcoli, A. D. Corso, and P. Giannozzi, Rev. Mod. Phys. **73**, 515 (2001).
[26] A. Y. Cheryakov, V. A. Somenkov, Y. S. Umanskii, S. S. Shil'shtein, and V. P. Yanchur, Izv. Vyssh. Uchebn. Zaved., Tsvetn. Metall. **14**, 140 (1971).
[27] W. Weber, P. Roedhammer, L. Pintschovius, W. Reichardt, F. Gompf, and A. N. Christensen, Phys. Rev. Lett. **43**, 868 (1979).
[28] A. I. Gusev, A. A. Rempel, and A. J. Magerl, *Disorder and Order in Strongly Nonstoichiometric Compounds: Transition Metal Carbides, Nitrides and Oxides* (Springer, Berlin, 2001).
[29] G. L. Bir and G. E. Pikus, *Symmetry and Deformation Effects in Semiconductors* (Nauka, Moscow, 1972).
[30] A. N. Christensen, A. Alamo, and J. P. Landesman, Acta Crystallogr. C **41**, 1009 (1985).
[31] D. Roundy, C. R. Krenn, M. L. Cohen, and J. W. Morris, Phys. Rev. Lett. **82**, 2713 (1999).
[32] R. Sanjines, M. Benkahoul, C. Sandu, P. E. Schmid, and F. Levy, Thin Solid Films **494**, 190 (2006).